Submitted to Chem. Phys., (Peter Saalfrank Festschrift), 8/14/2021, revised 11/4/2021

Influence of Supercell Size on Gas-Surface Scattering: A Case Study of CO Scattering from Au(111)

Ce Hu[1], Qidong Lin[1], Hua Guo[2, *], and Bin Jiang[1, *]

[1]*Hefei National Laboratory for Physical Science at the Microscale, Key Laboratory of Surface and Interface Chemistry and Energy Catalysis of Anhui Higher Education Institutes, Department of Chemical Physics, University of Science and Technology of China, Hefei, Anhui 230026, China*

[2]*Department of Chemistry and Chemical Biology, University of New Mexico, Albuquerque, New Mexico 87131, USA*

Keywords: energy dissipation, scattering, potential energy surfaces, surface science

*: corresponding authors: hguo@unm.edu, bjiangch@ustc.edu.cn

Abstract

We examine energy dissipation of impinging molecules (CO) on Au(111) using molecular dynamics on a machine learned high-dimensional potential energy surface (PES) describing the molecular and surface degrees of freedom. The PES was trained using a neural network method from density functional theory energies and gradients obtained with a relatively small supercell size, but it is capable of providing an accurate description of the molecule-surface interaction for larger supercells. This property allowed us to investigate the dependence of the dissipation dynamics on the supercell size. Our simulations indicated that the supercell size has essentially no effect on the direct scattered molecules, but the energy dissipation of the trapping molecules is significantly influenced by the size of the simulation cell. This observation has important implications in understanding dissipation at the gas-surface interface and their effects on various dynamics processes.

I. Introduction

Energy exchange between molecular species and metal surfaces represents an unavoidable issue in gas-surface encounters, because it can significantly impact the outcome. Adsorption, for example, is only possible if the impinging molecule loses some of its kinetic energy to enable its trapping on the surface. Desorption, on the other hand, is promoted by energy flow from the substrate to the adsorbate. As a result, a thorough understanding of the energy exchange mechanism and dynamics is of foundational importance in surface science.

It is well known that the energy carried by the impinging species can be either mechanically dissipated to the lattice vibration through an electronically adiabatic mechanism, or transferred to electron-hole pairs (EHPs) of metal surfaces via an electronically nonadiabatic mechanism.[1-5] While state-of-the-art molecular beam experiments provide detailed information about the energy conversion at gas-surface interfaces,[6-12] accurate theoretical modelling is often required for an in-depth understanding of the underlying mechanism and dynamics.[2,4,13-21] For example, it was very recently revealed by theory that adiabatic vibrational energy transfer from the molecule to surface phonons plays a non-negligible role in the scattering of highly vibrationally excited NO molecules from Au(111),[22,23] which provided valuable mechanistic insights into experimentally observed multi-quantum vibrational relaxation in the scattered NO. In another example, theoretical understanding of the physisorption and chemisorption wells for the current system and the associated energy transfer mechanisms [24,25] was instrumental in resolving experimentally observed

long relaxation time for vibrationally excited CO on the Au(111) surface.[26,27]

First-principles characterizations of gas-surface systems are largely based on plane wave density functional theory (DFT), which approximates an infinitely-extended surface with a thin slab within a periodically repeated supercell. In many of the earlier models, the surface degrees of freedom (DOFs) were usually neglected, resulting in adiabatic potential energy surfaces (PESs) of molecules interacting with static surfaces. This was necessary to avoid the construction of high-dimensional PESs that include the surface atoms, but such a rigid surface treatment is only valid for scattering of very light species such as H_2.[28] A number of models have been proposed to approximately to include the surface atom motion, as discussed in some details by two recent reviews.[19,20] For example, the surface oscillator (SO) model[29,30] was proposed to approximate the infinite surface vibration by a single harmonic oscillator. To include energy dissipation, rigid surface based PESs can be coupled with a generalized Langevin oscillator (GLO) model [31,32] as a thermal bath in terms of surface harmonic oscillators described by generalized Langevin equations. Saalfrank et al.[33-35] have further modified the SO model by introducing a linear coupling term to account for the barrier change due to surface oscillation and replaced the single surface oscillator by a set of GLOs. It was argued that it is better to include many GLOs approximately than treating a single oscillator exactly.[35] While the GLO model has been widely applied to many diatom-surface systems and Eley-Rideal processes,[36-41] it represents only a phenomenological approximation of the realistic surface lattice fluctuations. On the other hand, Jackson and coworkers[42-44] have carefully studied

lattice effects in CH_4 dissociation on various metal surfaces and concluded that a sudden lattice model is sufficient to provide quantitative corrections to the sticking probability. This sudden model however does not allow for energy exchange between the molecule and the surface. A modified GLO model has recently been proposed to better describe the change of the dissociation barrier caused by individual surface atom displacements,[45] but an atomistic characterization is still preferred for realistic simulations.

With increasing computational power, atomistic models have started to emerge in recent years. For example, surface motion has been explicitly taken into account in the *ab initio* molecular dynamics (AIMD) approach, an increasingly popular way of modeling gas-surface scattering dynamics that bypasses difficulties in constructing high-dimensional PESs.[17,46-49] However, the high computational costs in AIMD calculations have limited the slab model to adopt relatively small supercell sizes. This may lead to unphysical energy flow to and from the lattice, especially for indirect processes with long residence time on the surface.[50] For example, Novko *et al.* [51] used a 2×2 supercell with five metal layers in their AIMD (and AIMD with electronic friction) simulations of the adsorption of atomic N on Ag(111) and found that at low temperature the metal atoms in the top two layers are unphysically heated after 1~2 ps. This problem was alleviated by incorporating an additional thermal bath. To better describe the adiabatic energy dissipation for surface processes, Meyer and Reuter [52] proposed an embedding method, in which a small quantum mechanical (QM) region including the molecule and a regular surface slab is embedded in a phononic bath

consisting of thousands of metal (Me) atoms described by empirical force fields. This so-called QM/Me model was applied to the O_2 + Pd(100) system, revealing that a remarkable fraction (~80%) of the released chemisorption energy had propagated outside the QM region within 1.5 ps after O_2 dissociation.[53,54] These results suggest that the conventional size of the supercell in AIMD simulations may not be sufficient.

More recently, machine learning methods for fitting high-dimensional PESs have gradually matured. For example, the Behler-Parrinello neural network (BPNN) [55] and embedded atom neural network (EANN) [56] approaches have been successfully applied to generate DFT-based high-dimensional molecule-surface PESs including both molecular and surface DOFs in a supercell satisfying periodic boundary conditions.[22,25,57-66] Such analytical PESs are orders of magnitude faster than DFT calculations, thus enabling much more efficient MD simulations at the same level as AIMD. Importantly, the total energy in this atomistic type of NN PES is expressed as the sum of atomic energies accounting for modulations by their immediate environment. This offers scalability of such a PES in describing different supercell sizes, provided that the PES is well-trained, without sacrificing the accuracy of the interaction between surface atoms as in the QM/Me model.

In this work, we investigate the energy transfer dynamics of vibrationally excited CO scattering/trapping from Au(111) using a DFT-based EANN PES with a special focus on the influence of the supercell size. This system is chosen because of the earlier mentioned experimental work from the Wodtke group on the surprisingly long lifetime of vibrationally excited CO adsorbed on the Au(111) surface.[26] These authors

prepared the CO adsorbate on the Au surface via impinging gaseous CO(v=2) molecules and found desorbed CO(v=1) after more than 100 ps on the metal surface. This was unexpected as the vibrational lifetime of CO on metal surfaces, such as Cu and Pt, is known to be very short (ps) due to strong nonadiabatic coupling with EHPs.[67,68] The vibrational relaxation lifetime of CO(v=1) on Au(111) at 35 K was later directly measured as 49±3 ps,[69] significantly longer than those on other metal surfaces. Theoretically, Lončarić *et al.*[24] found that the Bayesian Error Estimation Functional with van der Waals corrections (BEEF-vdW) [70] results in a physisorption well, which has a much larger surface-molecule distance than that of the chemisorption well predicted by a semi-local functional, responsible for the long vibrational lifetime for CO(v=1) on Au(111). Huang *et al.*[25] later constructed a BPNN PES for CO interaction with Au(111) with the same BEEF-vdW, uncovering a metastable chemisorption well as well as a physisorption one. Quasi-classical trajectory (QCT) results on this PES qualitatively reproduced the experimental data of direct scattering and also provided a possible mechanism to the experimentally observed vibrational relaxation of CO(v=2) to CO(v=1).[26] More recently, the intricate interplay between weak physisorption and chemisorption of CO on Au(111) was revealed by temperature dependent molecular beam experiments and kinetic modeling.[27]

By refitting the same dataset with the EANN approach, we report here a new PES for this system that is more accurate and more efficient than the previous BPNN one. Interestingly, we find that this EANN PES constructed with a 3×3 supercell is capable of accurately predicting total energies for larger (*e.g.,* 4×4 and 5×5) supercells. With

this new PES, we simulate the scattering/trapping of vibrationally excited CO molecules on Au(111) under experimental conditions, and examine the energy dissipation dynamics with different supercell sizes. While the final energy distributions of the directly scattered molecules are insensitive to the size of the supercell, the trapping probability is found to increase with the increasing number of atoms in the supercell, suggesting that more energy is transferred into the lattice with a larger cell. This study thus gains insights into the energy transfer dynamics and offers guidance on the size dependence for future dynamical simulations of molecule-surface scattering.

II. Computational Details

A. Training Dataset

All the DFT forces and energies of points used for the EANN PES fitting were calculated via the Vienna *ab initio* simulation package (VASP) [71,72] with BEEF-vdW.[70] A slab model with four layers in a 3×3 unit cell was used to represent the Au(111) surface with the top two layers relaxed and a vacuum region of 16 Å in the Z direction. The kinetic energy in the plane wave basis set was truncated by 450 eV and the Brillouin zone was sampled via a 5×5×1 Monkhorst-Pack k-point mesh.[73] In this work, the source of training dataset consists of two portions of data points. We first collected 10766 DFT points extracted from the AIMD simulations reported in Ref. [25]. In addition, we used an efficient trajectory-free active learning strategy[74,75] to select additional molecule-free 1696 surface configurations for a more accurate description of surface phonons.

B. Neural Network Potential Energy Surface

The EANN approach proposed recently [56] was used to construct the CO+Au(111) PES, which is invariant with respect to permutation of identical nuclei. In the EANN framework, the total energy of the system is given as the sum of atomic energies, each of which is the output of an atomic neural network (ANN). Each atom can be considered as an impurity embedded in an environment composed of surrounding atoms and the embedded electron density at this atomic position is used as the structural descriptor for the ANN,[56] namely,

$$E = \sum_{i=1}^{N} E_i = \sum_{i=1}^{N} NN_i\left(\boldsymbol{\rho}^i\right). \tag{1}$$

In practice, a group of orbital-dependent density features $\{\rho_i\}$ can be generated by Gaussian-type orbitals (GTOs) centered at neighboring atoms,

$$\rho_i = \sum_{l_x,l_y,l_z}^{l_x+l_y+l_z=L} \frac{L!}{l_x!l_y!l_z!}\left(\sum_{j=1}^{N_c} c_j \varphi\left(\mathbf{r}_{ij}\right) f_c(r_{ij})\right)^2 \tag{2}$$

where N_c is the number of neighbor atoms within a cutoff radius (r_c), $f_c(r_{ij})$ is a cutoff function [76] to ensure that the contribution of neighbor atoms decay smoothly to zero at r_c. For metals, the cutoff function decays quickly with the internuclear distance as the interaction is largely short ranged. This is important below when we use the same ANNs to describe interactions in different supercell sizes. The GTO is given by,

$$\varphi\left(\mathbf{r}_{ij}\right) = x^{l_x} y^{l_y} z^{l_z} \exp\left(-\alpha\left|r - r_s\right|^2\right) \tag{3}$$

where $\mathbf{r}_{ij}$=(x, y, z) and r are Cartesian coordinates of the embedded atom i relative to atom j and its norm respectively; l_x, l_y and l_z represent the angular momentum components along each Cartesian axis, and the orbital angular momentum (L) is the

sum of them; α and r_s are parameters that determine the radial distribution of a GTO; c_j in Eq. (2) serves like an element-dependent expansion coefficient of an atomic orbital for atom j, which is optimized together with ANN parameters. Compared with the BPNN approach used in Ref. [25], EANN can be even more accurate and much more efficient (see below). This is because that the embedded density-like descriptors given in Eq. (2) not only implicitly incorporate three-body information of the local environment, but also scale linearly with respect to the number of neighboring atoms. The EANN approach has been successfully applied to constructing PESs,[56,64,77,78] and extended to learn dipoles and polarizabilities,[79] as well as electronic friction tensors of adsorbates on surfaces.[80]

As mentioned above, a total of 12462 points were used to fit the EANN PES, among which 90% of data points were used for training and the rest for testing. The hyperparameters of EANN are as follows: L=0, 1, and 2, r_c=7.6 Å, α=0.65 Å^{-2}, and r_s=0.00, 0.55, 1.10, 1.65, 2.20, 2.75, 3.30, 3.85, 4.40, 4.95, 5.50, 6.05, 6.60, 7.15 and 7.70 Å, which result in finally 39 embedded density features. Each ANN consists of two hidden layers with 40 and 60 neurons.

II.C. Quasi-Classical Trajectory Calculations

QCT calculations were performed with our in-house code heavily modified from VENUS.[81] The initial CO (v=2, J=0) molecule was launched from 8 Å above the Au(111) surface, whose orientation and position in the unit cell were sampled randomly. The diatomic molecule was treated as a vibrating rotor, whose internal energy was

calculated as a function of vibrational and rotational quantum numbers v and J semi-classically.[82] Following the experiment,[26] the incidence angle was fixed at θ=9° from the surface normal with the azimuthal angle randomly sampled. Surface atoms in the top two layers are allowed to move in QCT calculations, while the bottom two layers are fixed. The initial surface configurations were sampled via Andersen thermostat[83] with the experimental surface temperature (T_s = 300 K), but no thermostat was imposed when simulating the collisional processes. Each trajectory was propagated with a time step of 0.1 fs via the velocity Verlet algorithm. The trajectory was terminated and labeled as a "scattered" event when molecule-surface vertical distance exceeded 8.1 Å and the molecule velocity was pointing away from surface, or alternatively, a "trapped" event for the molecule staying on the surface at the end of a given propagation time. No dissociation event was observed at all in our calculations. Following the definition in Ref. [25], those scattered trajectories experiencing less than four bounces (whenever the molecular center changes its velocity direction at the surface) were referred as "direct scattered" (DS), otherwise they were considered to be first trapped and then desorb, namely "trapping desorption" (TD). Note that the maximum propagation time is 50 ps in this work, but some results terminated in a shorter propagation time are also present (see discussion below and the caption of each Figure). The statistical errors of QCT results were calculated via $\sigma=\sqrt{p(1-p)/N}$, where p is the probability in each condition and N is actual number of trajectories.

We note that there is evidence that the vibrational relaxation of CO on the Au(111) surface is dominated by the nonadiabatic mechanism,[24,25] especially for highly

vibrationally excited CO.[84] However, the simulations reported here will only focus on the adiabatic energy dissipation involving the surface motion without vibrational relaxation. Consequently, the results here should not be directly compared with experiment and should serve as a pure theoretical exercise. The dependence of EHP-induced energy dissipation on the size of the supercell is another open question. For example, increasing the size of the unit cell may effectively increase the number of interband excitations in the first Brillouin zone. Its influence on the strength of electronic friction tensor has been discussed by Box *et al.*[21], but is beyond the scope of this work.

III. Results and Discussion

Let us first check the overall reliability of the EANN PES. The root mean square errors (RMSEs) of the total energies and atomic forces for training and validation sets were found to be 3.37/4.14 meV and 9.38/10.71 meV/Å, respectively. The small RMSE for the validation set suggests no overfitting. These values are merely half of those reported on the previous BPNN PES in Ref. [25], namely 9.78 meV (energies) and 20.00 meV/Å (forces). Furthermore, even when the cutoff radius in EANN PES is 0.6 Å larger than that in the BPNN PES (to better capture the long-range interaction between CO and the gold surface), the former is ~7 times faster than the latter. Such a speedup largely arises from the linear scaling in computing the embedded density descriptors in EANN versus the quadratic scaling in computing atom centered symmetry functions in the BPNN approach. These results underscore the high accuracy

and high efficiency of the EANN PES.

To illustrate the fitting quality, we compare several representative one-dimensional cuts of the EANN PES with the DFT data. Specifically, when the center of mass (COM) of CO is fixed at the fcc/top site and the orientation of CO is parallel/perpendicular to the Au(111) surface within a 3×3 supercell (Figures 1a and 1b), the EANN PES faithfully reproduces the corresponding DFT points. The predicted adsorption energies and geometries of the physisorption and (metastable) chemisorption wells are in excellent agreement with those reported on the BPNN PES in Ref. [25]. More importantly, as the supercell is enlarged to a size of 4×4 (Figure 1c and 1d) and 5×5 (Figure 1e and 1f), the agreement between DFT energies and the EANN PES remains good, especially for parallel orientation. The EANN PES slightly underestimates the well depth for the metastable state of CO perpendicular to the fcc site within the 5×5 supercell. It should be emphasized that the EANN PES was trained with the data points generated from the 3×3 cell only, so this level of agreement is quite satisfactory. This excellent agreement confirms that the atomistic representation of PES allows us to expand the supercell size while keeping the accuracy of the PES with periodic boundary conditions. This is made possible by the "nearsightedness" of the interatomic interaction within the metal, which is shorter ranged than the cell size. Figure 1 also suggests that the molecule-surface interaction energy is largely converged for this system in the 3×3 supercell, from a static point of view. Further extending the cell size has a minor effect on the energetics.

Based on this EANN PES, we first calculated 5000 trajectories of CO(v=2)

scattering from Au(111) for different sizes of the slab with the same incident energy of E_{in}=0.32 eV up to 50 ps. We should note that the dynamics results on the EANN PES are very close to those on the BPNN PES (when used the 3×3 cell),[25] so their comparison is thus not discussed here.

In Figures 2 and 3, the distributions of vibrational energy, rotational energy, translational energy and scattering angles of the scattered CO in the DS and TD channels are compared, respectively, for different slab models. Consistent with the previous results,[25] the vibrational energy (E_{vib}^{f}) distributions are very narrow in both channels, regardless of cell sizes, suggesting strong vibrational elasticity in the absence of the electronic friction. This can be attributed to the large frequency mismatch between the CO vibration and surface phonons. Rotational energy (E_{rot}^{f}) distributions of two channels are similar, except for a slight increase in the proportion of high rotational energy in the DS channel. In comparison, a large discrepancy is found for the distributions of translational energy (E_{trans}^{f}) between the two channels, where the peak of the distribution is much lower in the TD (~0.05 eV) channel than that in the DS (~0.15 eV) channel. In addition, in contrast to a narrow and near specular angular distribution in the DS channel, the TD channel has a much broader angular distribution. These results suggest that the TD trajectories experience on average more prominent translational energy losses during the gas-surface encounters, due probably to the multiple contact between the molecule and the surface. Overall, there is no significant difference among these results with the three cell sizes, implying that the energy transfer occurring in a relatively short timescale can be reliably described by a small supercell.

Now let us turn to the trapping and desorption of the impinging CO. In Figure 4, we compare the trapping probability as a function of the incident energy obtained by QCT calculations (5000 trajectories launched at every incident energy) with that of experiment at T_s=273 K.[85] It is worth emphasizing that the experimental trapping probability at 100 K was measured by the King-Wells method and at other temperatures was fitted to a simple exponential function from time-of-flight distributions of the trapping-desorption component.[85] The residence time of CO on the clean Au(l11) surface was estimated to be less than ~1 s at 100 K,[85] a macroscopic time-scale that is impossible to model by QCT simulations. Here, the QCT calculations were performed with the 3×3 supercell and 10 ps of propagation time. So the comparison between theoretical and experimental trapping probability curves is qualitative and the theoretical results do follow the experimental trend quite well. However, this good agreement is deceiving as shown by results at E_{in}=0.32 eV with larger supercells and longer propagation times (see the blue diamond in Figure 4 and results in Figure 5). On one hand, for a given propagation time, the trapping probability increases with the cell size, indicating dependence of energy dissipation with the size of the cell used in the simulation. Even for the largest cell used in our study, the trapping probability is not yet converged. On the other hand, for a given cell size, the trapping probability decreases exponentially with the propagation time, as expected for a first-order trapping-desorption kinetics. Because of the limited propagation time (10 ps), the calculated trapping probability is apparently overestimated. The combination of the two factors suggests that any quantitative comparison of theoretical and experimental

trapping probabilities for molecular adsorption processes at solid surfaces should be taken with caution.

To further explore the influence of slab size on the energy dissipation and the resultant trapping/desorption dynamics, the mean kinetic energy of CO (Figure 6) and the surface temperature T_s (Figure 7) were monitored over time with the average of all trapped trajectories. Here, the surface temperature is approximated by the time average kinetic energy of the surface atoms. In Figure 6, a stronger fluctuation of the mean kinetic energy of CO in the 3×3 cell is found than in the 4×4 and 5×5 cells, especially during the first 2.5 ps, corresponding to the first a few bounces of the molecule right after the collision. This stronger fluctuation is likely a result of the smaller amount of surface atoms with which the incident CO molecule can exchange energy, which will accordingly cause more facile desorption (a lower trapping probability) of CO, as observed in Figure 5. In addition, we find in Figure 7 that in each case the surface temperature quickly elevates upon the gas-surface collision and then reaches to a relatively stable value. Interestingly, a larger cell tends to reach the equilibrium in a shorter period with an average T_s closer to the initial temperature (T_s=300 K), *e.g.*, $T_s \approx$ 358 K (3×3 cell) > $T_s \approx$ 334 K (4×4 cell) > $T_s \approx$ 322 K (5×5 cell). Our findings are consistent with the observations of Alducin and coworkers,[51] both of which indicate that the insufficient number of surface atoms used in the simulations will lead to the accumulation of most of the energy exchanged with the adsorbate, leading to unphysical heating of surface. This problems was even more severe in their calculations for the highly exothermic adsorption of atomic nitrogen on Ag(111),[51] where the substrate

temperature was increased by several hundred Kelvins during the fast adsorption process (~3.5 ps), if no thermal bath was imposed. These results clearly suggest that gas-surface energy dissipation is more adequately described when more surface atoms are explicitly involved during molecular dynamics simulations. It should be noted that energy transfer could also depend on the number of metal layers, but the current PES is less reliable to directly describe extra layers beyond the four-layer slab, due presumably to the lack of training data for relevant atomic structures. Another effective way to describe energy dissipation is to couple the lower layers of the surface with a thermostat, as performed in the work of Alducin *et al.*[51]and Groß.[86] Alternatively, we expect that an improved QM/Me model [52] with the QM part replaced by an analytical EANN PES would be useful and more efficient than the original version. Even better, a well-trained EANN PES in a sufficiently large supercell and more surface layers should offer a better description for the surface itself so that the empirical force field for the metal is unnecessary. This pure EANN approach will overcome the limit of the number of layers and the supercell explored in this work and allow for first-principles simulations of a much large slab size. Further investigations along this direction will be very promising.

Expanding the supercell also has an influence on the estimation of the residence lifetime of CO on Au(111). Following our previous work,[25] the lifetime (τ) is approximately extracted from the slope of the trapping probability *v.s.* propagation time in the logarithmic plot (Figure 5), assuming a first-order kinetics for desorption. It is found that the lifetime of trapped CO(v =2) increases monotonically from ~39 to ~54

ps as the slab size increases from 3×3 to 5×5, although the difference becomes smaller between 3×3 and 4×4 than between 4×4 and 5×5. It should be noted that this value cannot be directly compared with the measured vibrational relaxation lifetime of CO(v=1) on Au(111) at 35 K (49±3 ps) [69], because the realistic conditions are rather different, *e.g.*, the surface temperature, the initial state, and most importantly the extent departing from equilibrium (scattering *v.s.* pre-adsorption). Furthermore, the electron friction is ignored in this work. Nonetheless, our results point to the necessity of using a sufficiently large cell size in describing trapping dynamics, despite the higher computational cost.

IV. Conclusions

In this work, we report a scalable neural network PES for describing CO interaction with Au(111), based on a high-quality fit of tens of thousands of DFT data points. With the help of the atomistic representation of this EANN PES, we investigate the influence of the supercell size on the scattering of CO from Au(111) using a quasi-classical method. It is found that the distributions of vibrational energy, rotational energy, translational energy, scattering angle of the directly scattered CO molecules are largely insensitive to the supercell size. Whereas the calculated trapping probability always decreases with the propagation time, the absolute value increases with the increasing slab size, so as the estimated residence lifetime of the trapped CO molecule. Our analysis indicates that the surface may suffer from artificial heating upon the molecular collision if a small cell size is used, resulting in stronger fluctuation of surface atoms

and energy flow back to the molecule, and eventually lowering the trapping probability. Altogether, we argue that the commonly-used 3×3 supercell is sufficient to accurately capture the energy transfer dynamics in a relatively short timescale, but a larger supercell is required for describing the trapping dynamics, which requires a long propagation time.

Acknowledgement: This work is supported by National Natural Science Foundation of China (22073089 and 22033007) and The Fundamental Research Funds for Central Universities (WK2060000017). H. G. acknowledges support from the U.S. National Science Foundation (CHE-1951328). We thank the Supercomputing Center of USTC for providing high performance computation services.

References

[1] A.M. Wodtke, Chem. Soc. Rev. 45 (2016) 3641.

[2] M. Alducin, R. Díez Muiño, J.I. Juaristi, Prog. Surf. Sci. 92 (2017) 317.

[3] S. Monturet, P. Saalfrank, Phys. Rev. B 82 (2010) 075404.

[4] P. Saalfrank, G. Fuchsel, S. Monturet, J.C. Tremblay, T. Klamroth, in: R.D. Muino, H.F. Busnengo (Eds.), Dynamics of Gas-Surface Interactions, Springer, Heidelberg, 2013.

[5] P. Saalfrank, J.I. Juaristi, M. Alducin, M. Blanco-Rey, R. Díez Muiño, J. Chem. Phys. 141 (2014) 234702.

[6] O. Bünermann, H. Jiang, Y. Dorenkamp, A. Kandratsenka, S.M. Janke, D.J. Auerbach, A.M. Wodtke, Science 350 (2015) 1346.

[7] B.C. Kruger, N. Bartels, C. Bartels, A. Kandratsenka, J.C. Tully, A.M. Wodtke, T. Schafer, Journal of Physical Chemistry C 119 (2015) 3268.

[8] J. Geweke, P.R. Shirhatti, I. Rahinov, C. Bartels, A.M. Wodtke, J. Chem. Phys. 145 (2016) 054709.

[9] J. Werdecker, M.E. van Reijzen, B.-J. Chen, R.D. Beck, Phys. Rev. Lett. 120 (2018) 053402.

[10] H. Jiang, M. Kammler, F. Ding, Y. Dorenkamp, F.R. Manby, A.M. Wodtke, T.F. Miller, A. Kandratsenka, O. Bünermann, Science 364 (2019) 379.

[11] G.B. Park, B.C. Krüger, D. Borodin, T.N. Kitsopoulos, A.M. Wodtke, Rep. Prog. Phys. 82 (2019) 096401.

[12] J. Werdecker, B.-J. Chen, M.E. Van Reijzen, A. Farjamnia, B. Jackson, R.D. Beck, Physical Review Research 2 (2020) 043251.

[13] P. Saalfrank, Chem. Rev. 106 (2006) 4116.

[14] B. Jiang, H. Guo, J. Chem. Phys. 150 (2019) 180901.

[15] H. Guo, A. Farjamnia, B. Jackson, J. Phys. Chem. Lett. 7 (2016) 4576.

[16] P. Spiering, K. Shakouri, J. Behler, G.-J. Kroes, J. Meyer, J. Phys. Chem. Lett. 10 (2019) 2957.

[17] F. Nattino, D. Migliorini, G.-J. Kroes, E. Dombrowski, E.A. High, D.R. Killelea, A.L. Utz, J. Phys. Chem. Lett. 7 (2016) 2402.

[18] R. Moiraghi, A. Lozano, E. Peterson, A. Utz, W. Dong, H.F. Busnengo, J. Phys. Chem. Lett. 11 (2020) 2211.

[19] G.-J. Kroes, Phys. Chem. Chem. Phys. 23 (2021) 8962.

[20] S.P. Rittmeyer, V.J. Bukas, K. Reuter, Adv. Phys. X 3 (2018) 1381574.

[21] C.L. Box, Y. Zhang, R. Yin, B. Jiang, R.J. Maurer, JACS Au 1 (2021) 164.

[22] R. Yin, Y. Zhang, B. Jiang, J. Phys. Chem. Lett. 10 (2019) 5969.

[23] R. Yin, B. Jiang, Phys. Rev. Lett. 126 (2021) 156101.

[24] I. Lončarić, M. Alducin, J.I. Juaristi, D. Novko, J. Phys. Chem. Lett. 10 (2019) 1043.

[25] M. Huang, X. Zhou, Y. Zhang, L. Zhou, M. Alducin, B. Jiang, H. Guo, Phys. Rev. B 100 (2019) 201407(R).

[26] P.R. Shirhatti, I. Rahinov, K. Golibrzuch, J. Werdecker, J. Geweke, J. Altschäffel, S. Kumar, D.J. Auerbach, C. Bartels, A.M. Wodtke, Nat. Chem. 10 (2018) 592.

[27] D. Borodin, I. Rahinov, P.R. Shirhatti, M. Huang, A. Kandratsenka, D.J. Auerbach, T.L. Zhong, H. Guo, D. Schwarzer, T.N. Kitsopoulos, A.M. Wodtke, Science 369 (2020) 1461.

[28] G.-J. Kroes, Prog. Surf. Sci. 60 (1999) 1.

[29] J.C. Tully, Annu. Rev. Phys. Chem. 31 (1980) 319.

[30] M. Hand, J. Harris, J. Chem. Phys. 92 (1990) 7610.

[31] J.C. Tully, J. Chem. Phys. 73 (1980) 1975.
[32] H.F. Busnengo, W. Dong, A. Salin, Phys. Rev. Lett. 93 (2004) 236103.
[33] M. Dohle, P. Saalfrank, Surf Sci. 373 (1997) 95.
[34] M. Dohle, P. Saalfrank, T. Uzer, J. Chem. Phys. 108 (1998) 4226.
[35] M. Dohle, P. Saalfrank, T. Uzer, Surf Sci. 409 (1998) 37.
[36] M. Alducin, R. Díez Muiño, H.F. Busnengo, A. Salin, Phys. Rev. Lett. 97 (2006) 056102.
[37] I. Goikoetxea, J. Beltran, J. Meyer, J.I. Juaristi, M. Alducin, K. Reuter, New J. Phys. 14 (2012) 013050.
[38] L. Martin-Gondre, M. Alducin, G.A. Bocan, R. Díez Muiño, J.I. Juaristi, Phys. Rev. Lett. 108 (2012) 096101.
[39] M. Blanco-Rey, E. Díaz, G.A. Bocan, R. Díez Muiño, M. Alducin, J.I. Juaristi, J. Phys. Chem. Lett. 4 (2013) 3704.
[40] L. Diekhoner, D.A. Butler, A. Baurichter, A.C. Luntz, Surf. Sci. 409 (1998) 384.
[41] F. Nattino, O. Galparsoro, F. Costanzo, R. Díez Muiño, M. Alducin, G.-J. Kroes, J. Chem. Phys. 144 (2016) 244708.
[42] S. Nave, B. Jackson, Phys. Rev. Lett. 98 (2007) 173003.
[43] S. Nave, B. Jackson, J. Chem. Phys. 130 (2009) 054701.
[44] S. Nave, A.K. Tiwari, B. Jackson, J. Chem. Phys. 132 (2010) 054705.
[45] X. Zhou, B. Jiang, J. Chem. Phys. 150 (2019) 024704.
[46] A. Groß, Phys. Rev. Lett. 103 (2009) 246101.
[47] F. Nattino, C. Díaz, B. Jackson, G.-J. Kroes, Phys. Rev. Lett. 108 (2012) 236104.
[48] D. Novko, M. Blanco-Rey, J.I. Juaristi, M. Alducin, Phys. Rev. B 92 (2015) 201411(R).
[49] X. Zhou, B. Kolb, X. Luo, H. Guo, B. Jiang, J. Phys. Chem. C 121 (2017) 5594.
[50] F. Nattino, F. Costanzo, G.-J. Kroes, J. Chem. Phys. 142 (2015) 104702.
[51] D. Novko, I. Lončarić, M. Blanco-Rey, J.I. Juaristi, M. Alducin, Phys. Rev. B 96 (2017) 085437.
[52] J. Meyer, K. Reuter, Angew. Chem. Int. Ed. 53 (2014) 4721.
[53] V.J. Bukas, K. Reuter, Phys. Rev. Lett. 117 (2016) 146101.
[54] V.J. Bukas, K. Reuter, J. Chem. Phys. 146 (2017) 014702.
[55] J. Behler, M. Parrinello, Phys. Rev. Lett. 98 (2007) 146401.
[56] Y. Zhang, C. Hu, B. Jiang, J. Phys. Chem. Lett. 10 (2019) 4962.
[57] B. Kolb, X. Luo, X. Zhou, B. Jiang, H. Guo, J. Phys. Chem. Lett. 8 (2017) 666.
[58] Q. Liu, X. Zhou, L. Zhou, Y. Zhang, X. Luo, H. Guo, B. Jiang, J. Phys. Chem. C 122 (2018) 1761.
[59] Y. Zhang, X. Zhou, B. Jiang, J. Phys. Chem. Lett. 10 (2019) 1185.
[60] K. Shakouri, J. Behler, J. Meyer, G.-J. Kroes, J. Phys. Chem. Lett. 8 (2017) 2131.
[61] N. Gerrits, K. Shakouri, J. Behler, G.-J. Kroes, J. Phys. Chem. Lett. 10 (2019) 1763.
[62] M. del Cueto, X. Zhou, L. Zhou, Y. Zhang, B. Jiang, H. Guo, J. Phys. Chem. C 124 (2020) 5174.
[63] S. Wille, H. Jiang, O. Bünermann, A.M. Wodtke, J. Behler, A. Kandratsenka, Phys. Chem. Chem. Phys. 22 (2020) 26113.
[64] L. Zhu, Y. Zhang, L. Zhang, X. Zhou, B. Jiang, Phys. Chem. Chem. Phys. 22 (2020) 13958.
[65] E. Dombrowski, E. Peterson, D. Del Sesto, A.L. Utz, Catal. Today 244 (2015) 10.
[66] A. Serrano Jiménez, A. Sánchez Muzas, Y. Zhang, J. Ovcar, B. Jiang, I. Lončarić, J. Juaristi, M. Alducin, J. Chem. Theory Comput. 17 (2021) 4648.
[67] J.D. Beckerle, R.R. Cavanagh, M.P. Casassa, E.J. Heilweil, J.C. Stephenson, J. Chem. Phys. 95 (1991) 5403.

[68] M. Morin, N.J. Levinos, A.L. Harris, J. Chem. Phys. 96 (1992) 3950.
[69] S. Kumar, H. Jiang, M. Schwarzer, A. Kandratsenka, D. Schwarzer, A.M. Wodtke, Phys. Rev. Lett. 123 (2019) 156101.
[70] J. Wellendorff, K.T. Lundgaard, A. Møgelhøj, V. Petzold, D.D. Landis, J.K. Nørskov, T. Bligaard, K.W. Jacobsen, Phys. Rev. B 85 (2012) 235149.
[71] G. Kresse, J. Furthmuller, Phys. Rev. B 54 (1996) 11169.
[72] G. Kresse, J. Furthmuller, Comp. Mater. Sci. 6 (1996) 15.
[73] H.J. Monkhorst, J.D. Pack, Phys. Rev. B 13 (1976) 5188.
[74] Q. Lin, Y. Zhang, B. Zhao, B. Jiang, J. Chem. Phys. 152 (2020) 154104.
[75] Q. Lin, L. Zhang, Y. Zhang, B. Jiang, J. Chem. Theory Comput. 17 (2021) 2691.
[76] J. Behler, J. Chem. Phys. 134 (2011) 074106.
[77] J.P. Perdew, K. Burke, M. Ernzerhof, Phys. Rev. Lett. 77 (1996) 3865.
[78] X. Zhou, Y. Zhang, H. Guo, B. Jiang, Phys. Chem. Chem. Phys. 23 (2021) 4376.
[79] Y. Zhang, S. Ye, J. Zhang, C. Hu, J. Jiang, B. Jiang, J. Phys. Chem. B 124 (2020) 7284.
[80] Y. Zhang, R.J. Maurer, B. Jiang, J. Phys. Chem. C 124 (2020) 186.
[81] X. Hu, W.L. Hase, T. Pirraglia, J. Comput. Chem. 12 (1991) 1014.
[82] W.L. Hase, in: N.L. Alinger (Ed.), Encyclopedia of Computational Chemistry, Wiley, New York, 1998, p. 399.
[83] H.C. Andersen, J. Chem. Phys. 72 (1980) 2384.
[84] R.J.V. Wagner, N. Henning, B.C. Krüger, G.B. Park, J. Altschäffel, A. Kandratsenka, A.M. Wodtke, T. Schäfer, J. Phys. Chem. Lett. 8 (2017) 4887.
[85] C.T. Rettner, J. Chem. Phys. 99 (1993) 5481.
[86] A. Groß, Catal. Today 260 (2016) 60.

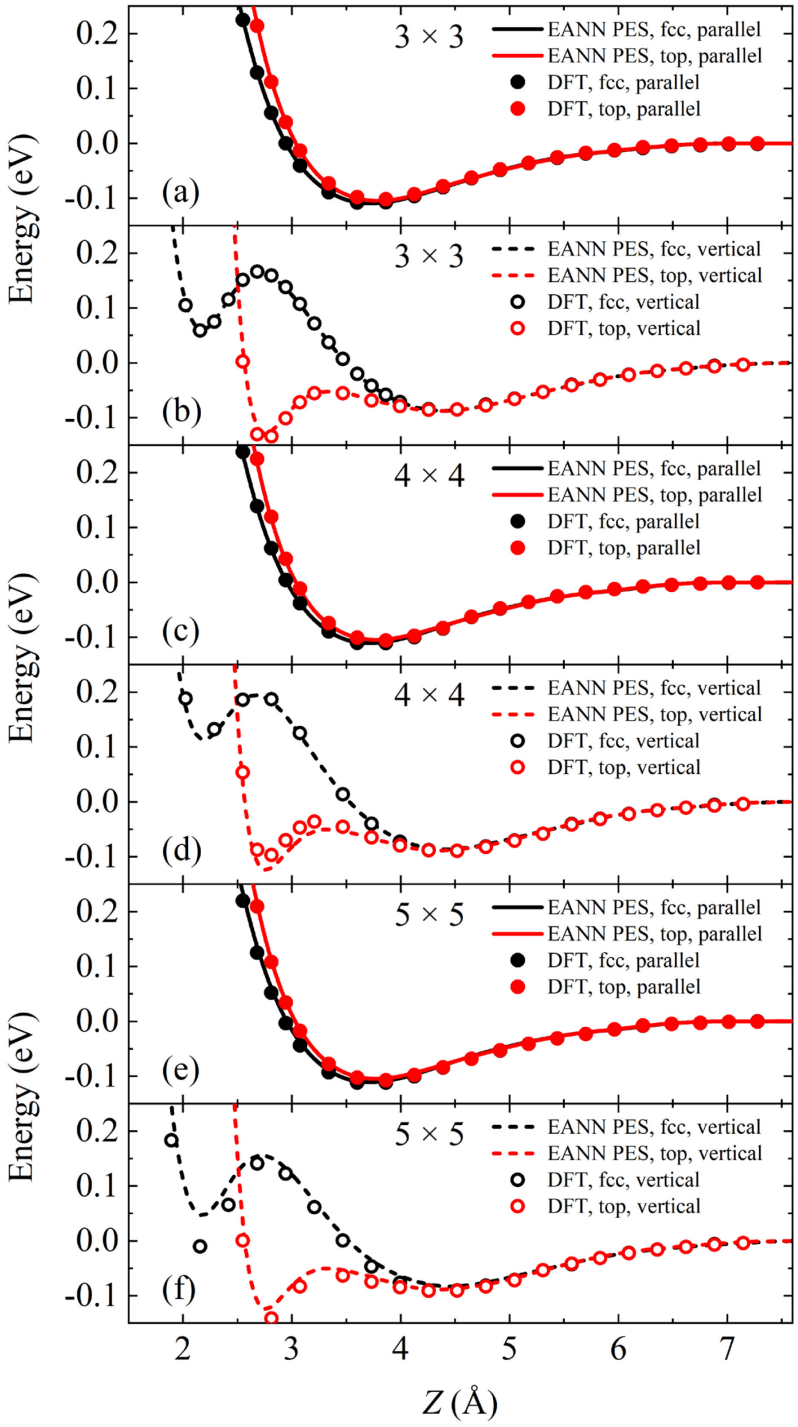

Figure 1. One-dimensional cuts of the EANN PES as a function of Z (the distance between the CO center of mass and surface) for CO at fcc/top sites and parallel/perpendicular to the Au(111) surface, compared with DFT data with 3×3 (a-b), 4×4 (c-d), and 5×5 (e-f) supercells.

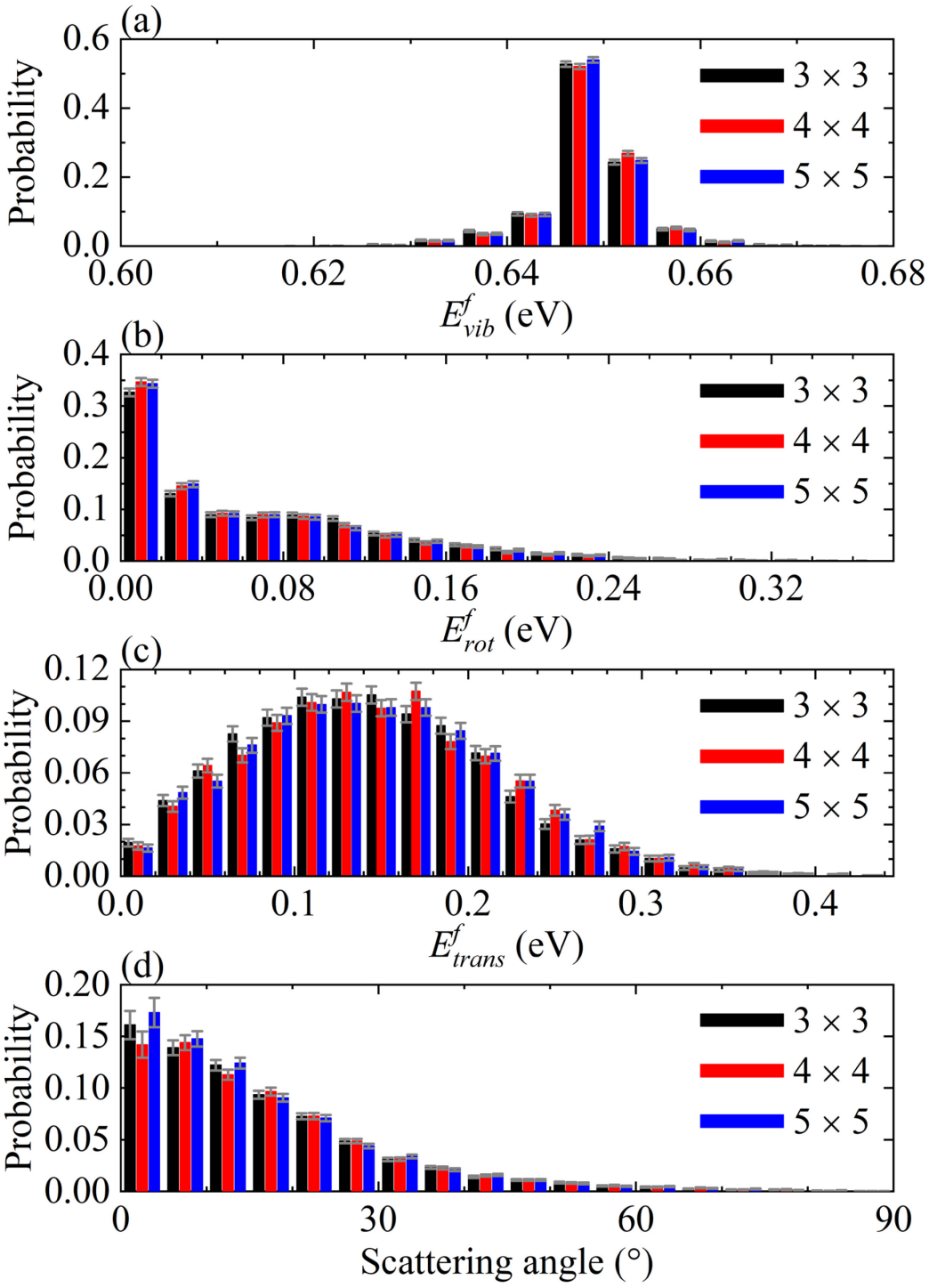

Figure 2. Distributions of (a) vibrational energy (E^f_{vib}), (b) rotational energy (E^f_{rot}), (c) translational energy (E^f_{trans}) and (d) scattering angle of the directly scattered (DS) CO for three different slab sizes, at E_{in}=0.32 eV and T_s=300 K.

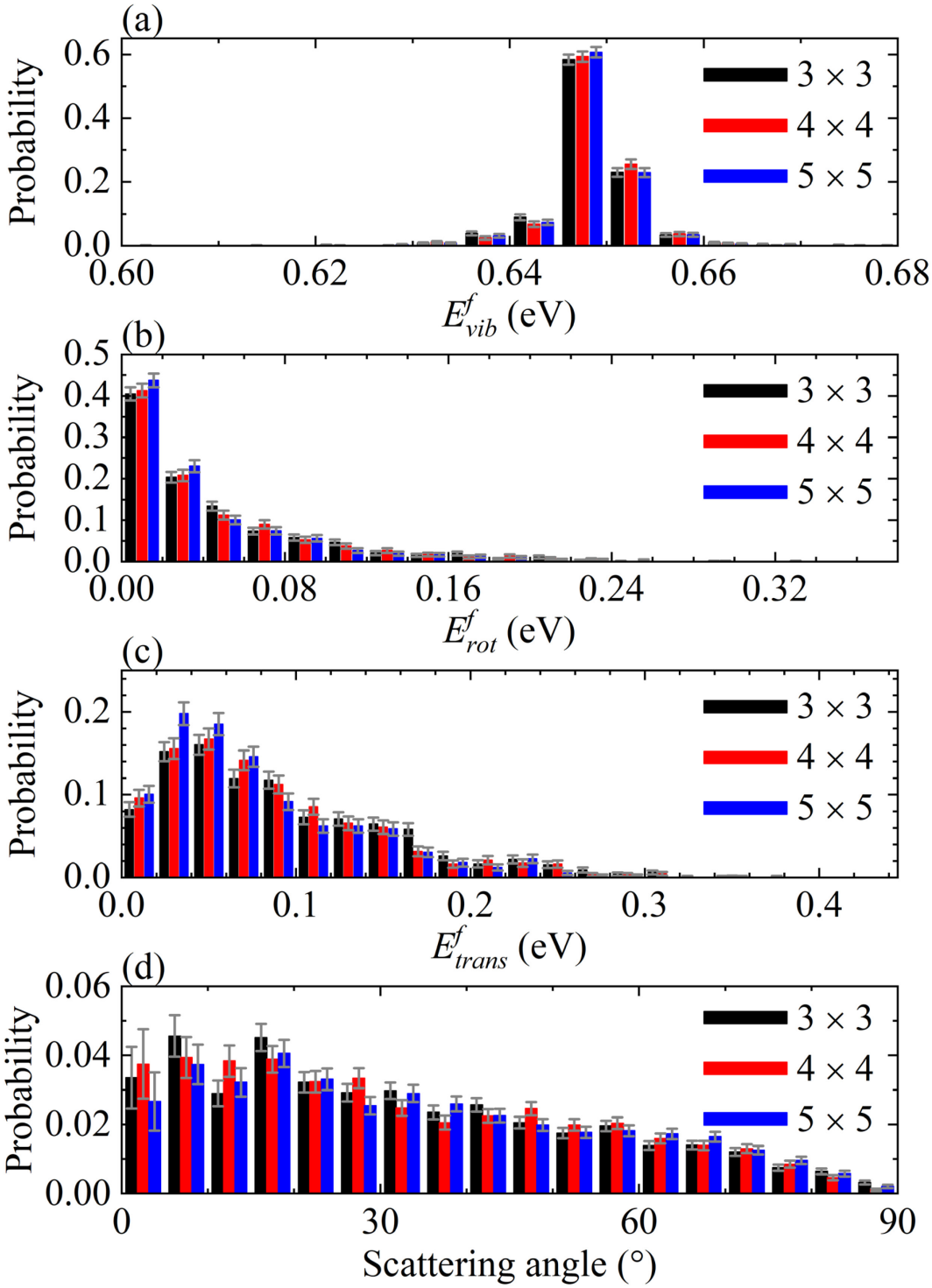

Figure 3. The same as Figure 2 but for the trapping desorption (TD) channel.

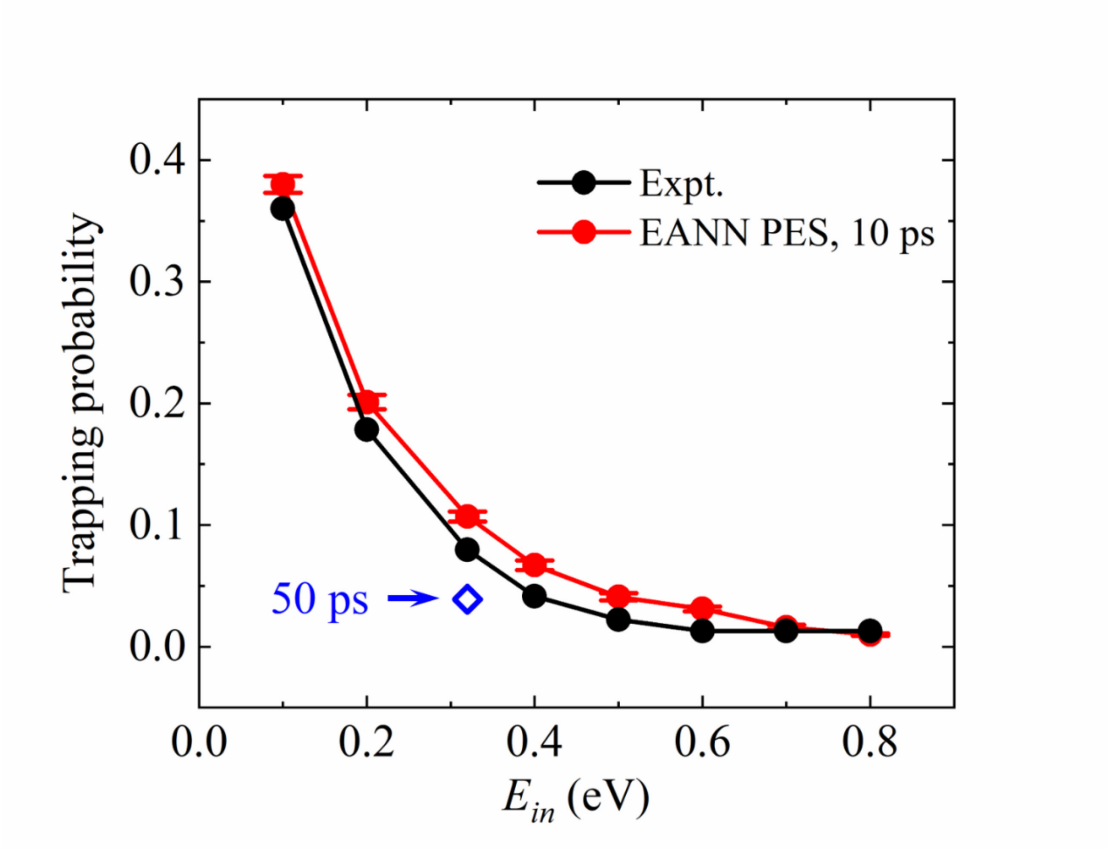

Figure 4. Qualitative comparison of the trapping probabilities as a function of incident energy (E_{in}) calculated on the EANN PES with the 3×3 supercell for 10 ps propagation (T_s=300 K) and measured in experiment (T_s=273 K).[85] The blue diamond represents the trapping probability when the propagation time is extended to 50 ps at E_{in}=0.32 eV.

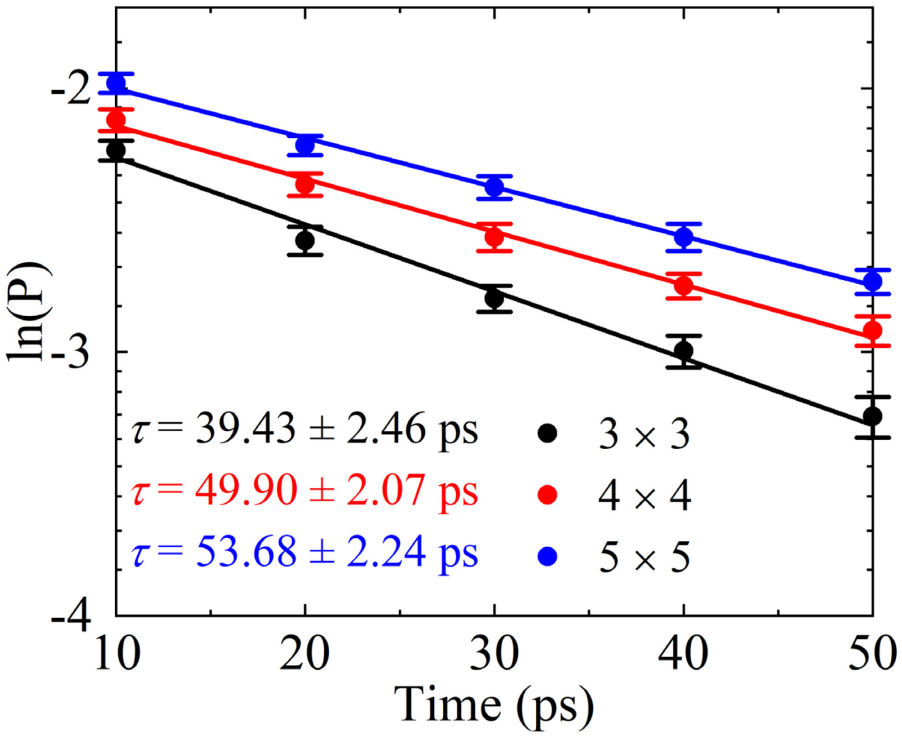

Figure 5. Fraction of CO molecules trapped on the surface as a function of time for different slab sizes, along with the residence lifetime (τ) estimated by the slope of each fitted line.

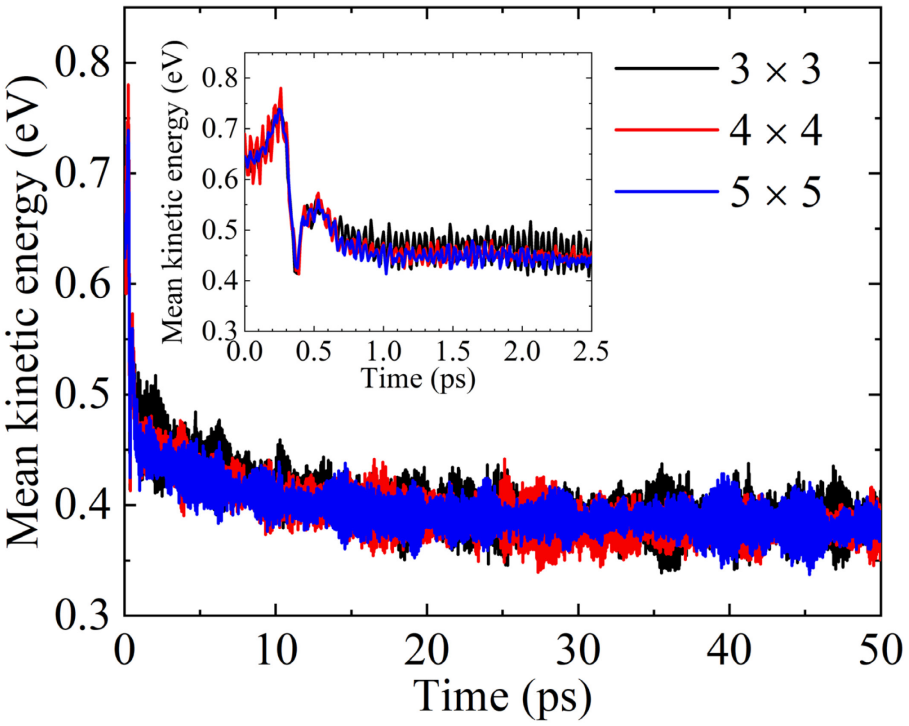

Figure 6. Mean kinetic energy of CO against time for different slab sizes and the inset amplifies the first 2.5 ps.

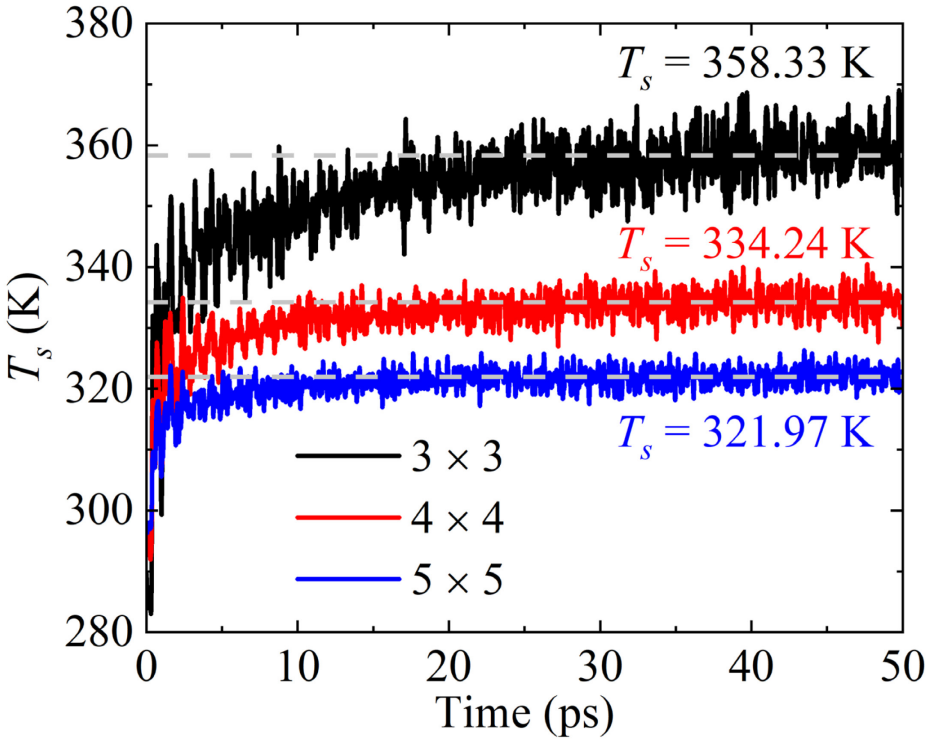

Figure 7. Variation of surface temperature (T_s) over time in different slab sizes with an initial T_s of 300 K. The gray dashed lines guide the eyes for seeing the equilibrium temperature in each case.